Investigation of Alloy 600 Welding Parameters

Results of experimental study followed by a heat model analysis provide the bases for conclusions, hypotheses and further study

BY S. S. GLICKSTEIN, E. FRIEDMAN AND W. YENISCAVICH

ABSTRACT. A series of bead-on-plate welds have been made with Alloy 600, varying the current, arc gap, torch speed, shielding gas, and electrode configuration. The width, depth, and area of the melt zone were then correlated to these parameter variations. In addition, the temperature at selected points on the weld plate was measured as a function of time and compared to calculations using a finite element heat conduction computer program.

Introduction

As part of an effort to describe the effects of welding variables on Alloy 600, bead-on-plate welds were performed and the melt zone analyzed. While similar studies of this type have been reported in the past, none have dealt systematically with Alloy 600. The welding variables considered in this program included weld current, arc gap spacing, welding speed, shielding gas, and electrode configuration.

To assess the capabilities of a finite element thermal analysis of the welding process, Chromel-alumel thermocouples were attached to various points on the weld plates to record temperature changes that occurred during and after the heat was applied. The numerical analysis can be a valuable and relatively inexpensive tool for performing parametric studies of the effects on the transient thermal cycle of various weldment characteristics; e.g., weld speed, magnitude and distribution of the heat source, weld joint geometry and heat sink contributions of adjacent fixturing or structure. An accurate determination of the temperature transients is required for further numerical studies of residual stresses and distortions developed as a result of welding. The results of the temperature-time relationship of the welded plates has helped to demonstrate the usefulness as well as the deficiencies of this analytical description of the welding process.

Experiment

Welds were made automatically using a gas tungsten-arc welding torch attached to a side beam welding fixture. The material described in Table 1 consisted of 2 × 2 × ¼ in. Alloy 600 coupons machined from 0.300 in. thick hot rolled plate. The plates were held in place by four set screws as shown in Fig. 1a in order to eliminate the external heat sink that a clamping mechanism would have introduced.

The electrodes used throughout this study were precision ground 3/32 in. diam., 2% thoriated tungsten and had a tip with a 28 ± 4 deg included angle and a 0.018 ± 0.003 in. flat tip, except when tip variations were intentionally made. A number 6 gas cup was used with an argon gas flow rate of 15 cfh. The electrode extended beyond the cup 3/16 in.

Chromel-alumel thermocouples were spot welded to various points on the top and bottom surface of the plate as shown in Fig. 1b and the signals recorded with a four channel chart recorder.

Weld current and voltage were simultaneously recorded during welding on a Honeywell chart recorder. Since the IR drop in the line cable and electrode was included in the voltage measurement, an additional test was run to estimate this voltage drop. After the arc was initiated, the voltage V_b, between the electrode and the baseplate was measured for various

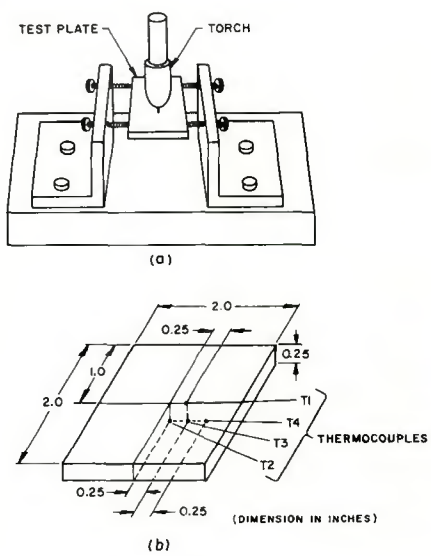

Fig. 1 — Experimental arrangement for holding the weld plate and thermocouple locations

The authors are associated with the Bettis Atomic Power Laboratory operated for the U.S. Atomic Energy Commission by Westinghouse Electric Corporation, Pittsburgh, Pennsylvania.

Paper to be presented at the 56th AWS Annual Meeting, Cleveland, Ohio, April 21-25, 1975.

Table 1 — Chemical Analysis of Alloy 600 (Heat LC 51880) Wt. %

Ni	Cr	Fe	Mn	C	Cu	Si	Co	S	P	Al	Ti	B	Mg
76.14	15.27	7.56	0.34	0.026	0.04	0.20	0.08	0.005	0.018	0.16	0.26	0.005	<0.01

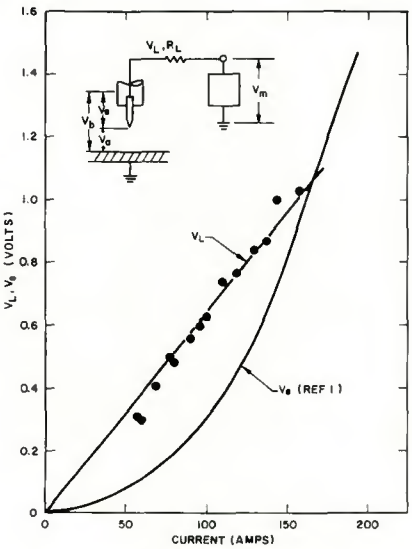

Fig. 2 — Voltage drop in line cable V_L ($V_L = V_m - V_b$) and electrode V_e, as a function of welding current

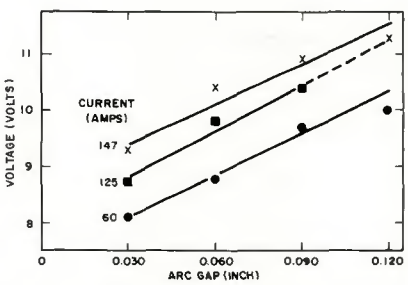

Fig. 4 — Recorded Voltage of stationary arc welds with increasing arc gap. Arc duration = 10 s

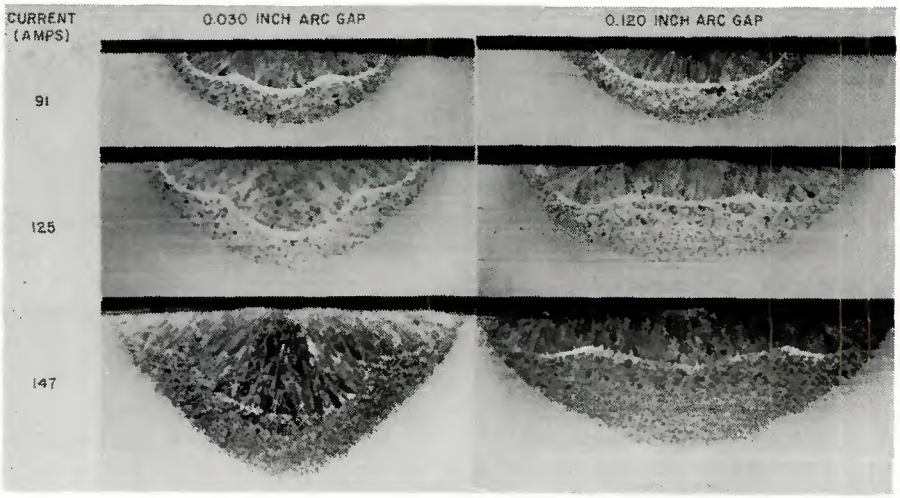

Fig. 3 — Cross sections of stationary arc welds on 2 × 2 × ¼ in. Alloy 600 plate. Arc duration = 10 s. X10, reduced 48%

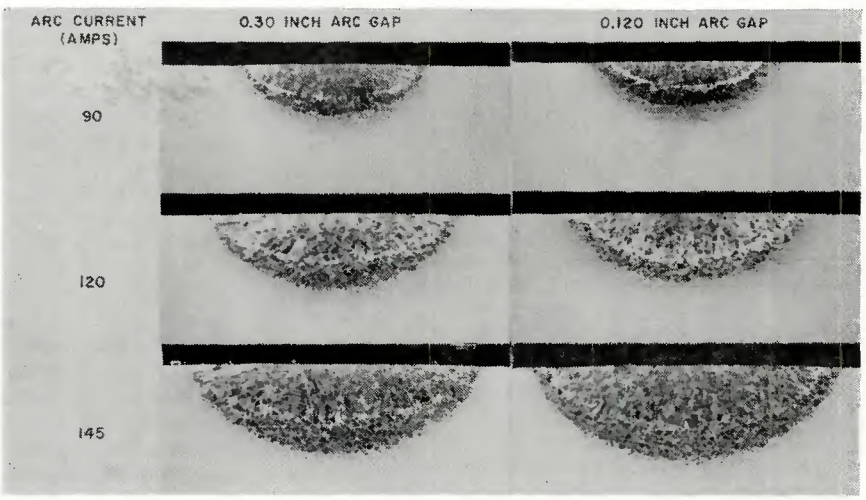

Fig. 5 — Cross sections of moving arc welds on 2 × 2 × ¼ in. Alloy 600 plate. Travel speed, 5 ipm. X10, reduced 43%

current settings. The difference between the voltmeter measurement V_b, and that recorded by the chart recorder V_m was equivalent to V_L, the IR loss in the line. The results of this test are shown in Fig. 2.

While this result is not unusual, nor surprising, it is not always considered by investigators who attempt to compare one set of welding parameters to another. For example, comparisons are sometimes made between welds for the same heat input, where heat input is taken as the product of the current and voltage. Such voltage measurements normally include the line and electrode voltage drop which, in many cases is not independently measured and can be quite significant. The precise point at which the voltage is measured is rarely defined and is thus not a very useful term to describe the input energy available to the weldment. Chihoski (Ref. 1) has reported a detailed study of these effects on voltage and from his work the potential drop in the electrode employed in this study was estimated. This is noted in Fig. 2 as V_e. The voltage measurements quoted in this report were read from the chart recorder normally employed during welding and thus included the IR drop in the line (V_L), and electrode (V_e), and arc (V_a).

After the welds were made, the plates were sectioned and electrolytically etched with a 10% chromic acid solution. The use of chromic acid instead of the usual phosphoric solution clearly distinguished the melt zone, which appeared to be outlined by a distinct white border. Width, depth, and area measurements were then made on 10X photographs of the weld. A planimeter was employed to determine the melt zone area.

The data in many cases, showed significant scatter which was due to the difficulty in determining the exact melt zone. In other cases, the puddle solidified above the original surface level of the plate. This was attributed to shrinkage and warping of the weld plate. The depth of penetration was therefore difficult to establish precisely and had to be approximated. The voltage varied a few tenths of a volt during many runs and at other times did not reach equilibrium. In such cases, comparisons were made be-

tween measurements at the completion of the weld. Thus, the absolute numbers presented in this report must be examined with care, but the trends observed from run to run are significant and reveal a number of interesting observations which will be discussed in the following sections.

Results

Stationary Arc

The initial set of experiments consisted of a stationary arc held in position for 10 seconds. A summary of the resultant width, depth, area, voltage and peak temperatures obtained for the various weld conditions are given in Table 2. Typical cross section configurations of the welds are shown in Fig. 3. An interesting feature of the weld cross section is the humped configuration that was obtained at the bottom of the pool for the stationary arc weld. Such a configuration was not expected from a normally distributed heat source incident on a plate. The effects of surface tension, arc jet forces, or the Lorentz force due to the current in the weld pool may each help to explain such a phenomenon. Ishizaki (Ref. 2) had observed a similar effect, and has particularly emphasized the importance of interfacial tension of the molten metal in producing a distorted weld puddle configuration. His explanation for the phenomenon is attributed to the motion of the weld pool induced by differences in the surface tension in the molten puddle. Ishizaki's studies showing the various penetration patterns that were obtained for paraffin and stearic acid heated by a point heat source such as a soldering iron, are similar to the results obtained with Alloy 600.

The area, width, and depth of the weld puddle were strongly dependent on the current. These parameters were essentially invariant with changes in arc gap at currents below 100 A, but at higher currents there was a significant decrease in the depth of penetration as the arc gap increased. The arc voltage increased approximately 0.25 volts per 0.010 in. increase in arc gap, as shown in Fig. 4. Thus, while the nominal arc power, typically quoted as V × I increased with arc gap spacing, the total heat input to the material, measured by the area of the melt zone and the temperature of the plate at T-2 and T-3, remained approximately constant or showed a decrease at high current. The temperature increase on the top surface of the plate at T-1 with increasing arc gap, as shown in Table 2, is attributed to a widening of the heat source incident on the surface of the weld plate.

Moving Arc

The results of the moving arc experiments are shown in Tables 3 and 4, and typical cross sections of the welds are shown in Fig. 5. From the tables it is noted that increasing the speed from 5 ipm to 10 ipm reduces the effective input heat which

Table 2 — Results of Stationary Arc Welds for 10 Seconds Duration, with Arc Gaps of 30, 60, 90 and 120 Mils for Each of Four Current Levels Shown (a)

	Current = 60 A				Current = 91 A				Current = 215 A				Current = 147 A			
Arc gap, mils	30	60	90	120	30	60	90	120	30	60	90	120	30	60	90	120
Width in.	—	0.158	0.164	0.152	0.234	0.234	0.220	0.220	0.30	0.35	0.34	0.35	0.386	0.412	0.434	0.470
Depth, in.	—	0.025	0.022	0.022	0.048	0.038	0.036	0.040	0.086	0.080	0.055	0.050	0.125	0.100	0.086	0.70
Width/depth	—	6.36	7.45	6.90	4.87	6.16	6.19	5.5	3.5	4.4	6.1	7.0	3.08	4.12	5.17	6.70
Area × 100, sq. in.	—	0.30	0.32	0.20	0.685	0.665	0.684	0.715	1.58	1.67	1.49	1.48	3.26	2.82	2.52	2.35
Voltage, V	8.1	8.8	9.7	10.0	8.5	9.5	—	—	8.7	9.8	10.4	—	9.3	10.4	10.9	11.3
Peak temperatures, F, for thermocouples T-1 to T-4 (see Fig. 1b)																
T-1	642	517	748	732	878	900	1009	—	1336	1554	1816	1728	1644	2077	—	1728
T-2	948	1074	1074	1074	1162	1336	1242	1242	1610	1642	1685	1640	1948	1860	1864	1728
T-3	594	668	704	682	792	813	900	778	1032	1242	1293	1206	1544	1816	—	1544
T-4	250	294	346	334	377	377	442	403	534	550	550	530	770	943	550	770

(a) The uncertainty in the temperature is estimated ±100 F. The voltage varied during welding and the values shown are average values taken toward the end of the 10 second weld period.

Table 3 — Results of Moving Arc Welds at V = 5 ipm and Arc Gaps of 30, 60, 90 and 120 Mils for Each of Four Current Levels Shown (a)

	Current = 58 A				Current = 90 A				Current = 120 A				Current = 145 A			
Arc gap, mils	30	60	90	120	30	60	90	120	30	60	90	120	30	60	90	120
Width, in.	0.108	0.095	0.066	0.090	0.190	0.172	0.18	0.168	0.265	0.258	0.253	0.240	0.30	0.30	0.32	0.31
Depth, in.	0.023	0.014	0.010	0.016	0.040	0.041	0.040	0.028	0.056	0.059	0.056	0.055	0.065	0.074	0.074	0.078
Width/depth	4.7	6.8	6.6	5.69	4.75	4.2	4.5	6.0	4.74	4.37	4.51	4.37	4.62	4.06	4.33	3.98
Area × 100, sq. in.	0.20	0.11	0.056	0.085	0.58	0.52	0.52	0.32	1.04	1.03	1.01	0.97	1.54	1.68	1.60	1.68
Voltage, V	7.6	7.5	8.6	8.3	8.4	8.7	8.5	9.9	8.8	9.7	10.1	10.6	9.6	10.2	10.8	11.4
Peak temperatures, F, for thermocouples T-1 to T-3 (see Fig. 1b)																
T-1	440	420	490	475	800	650	740	940	835	935	1075	1075	900	1205	1445	1424
T-2	725	725	725	725	1050	1075	1055	1120	1380	1355	1380	1380	1555	1620	1620	1640
T-3	475	485	445	445	704	725	655	780	800	780	860	945	770	1140	1120	1205

(a) The uncertainty in the temperature is estimated +100 F. The voltage varied during welding and the values shown are the average values taken toward the end of the run.

Table 4 — Results of Moving Arc Welds at V = 10 Ipm and Arc Gaps of 30, 60, 90 and 120 Mils for Each of Four Current Levels Shown (a)

Arc gap, mils	Current = 59 A				Current = 91 A				Current = 119 A				Current = 145 A			
	30	60	90	120	30	60	90	120	30	60	90	120	30	60	90	120
Width, in.	0.10	0.081	0.05	—	0.153	0.145	0.135	0.118	0.21	0.20	0.195	.185	0.24	0.24	0.24	0.24
Depth, in.	0.02	0.014	0.007	—	0.033	0.029	0.022	0.020	0.039	0.042	.040	.037	0.048	0.050	0.050	0.045
Width/depth	5.0	6.1	4.3	—	4.6	5.0	6.1	5.9	5.6	4.8	4.8	5.0	5.0	4.8	4.9	5.3
Area × 100, sq. in.	0.162	0.07	—	—	0.36	0.30	0.23	0.16	0.60	0.61	0.56	0.47	0.79	0.89	0.90	0.84
Voltage, V	8.0	8.3	9.5	—	8.7	9.5	9.8	10.3	9.3	10.0	10.5	10.8	10.0	10.7	11.3	—
Peak temperatures, F, for thermocouples T-1 to T-4 (see Fig. 1b)																
T-1	325	320	325	420	465	510	560	705	650	585	880	750	965	850	1030	780
T-2	475	335	335	—	680	705	670	705	890	955	955	900	1075	1160	1110	1110
T-3	290	320	325	345	445	455	445	265	585	573	541	615	704	815	730	715
T-4	—	200	230	190	245	265	500	270	325	335	300	350	390	425	410	373

(a) The uncertainty in the temperature is estimated ±100 F. The voltage varied during welding and the values shown are the average values taken toward the end of the run.

results in smaller weld puddle dimensions. The effects of the other welding parameters on the weld puddle discussed in the following paragraph were similar for both the 5 ipm and 10 ipm welding speeds considered. As in the stationary arc there is a strong dependence of the melt zone geometry on current. But for the moving arc at low current, the width, depth, and area of the weld puddle decreased as the arc gap increased, contrary to an invariant effect observed with the stationary arc at low current. Only at the higher currents did the puddle geometry become insensitive to the gap spacing. It is interesting to note that where the puddle geometry was relatively invariant to the arc gap spacing for the stationary and moving arc, the total heat input as measured by the thermocouples and melt area, was approximately the same.

The measured change in voltage with change in arc length is +0.15 to +0.20 V per 0.010 in. increase in arc length. While increasing the arc gap increased the nominal input power (V × I), as with the stationary arc, the input heat remained approximately constant.

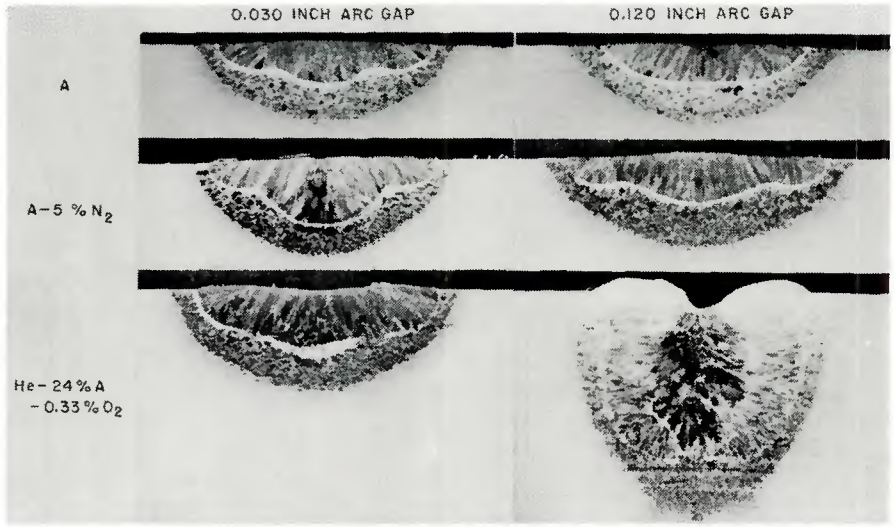

Fig. 6 — Cross sections of stationary welds made with variable shielding gases. I = 90 A. Arc duration = 10 s. X10, reduced

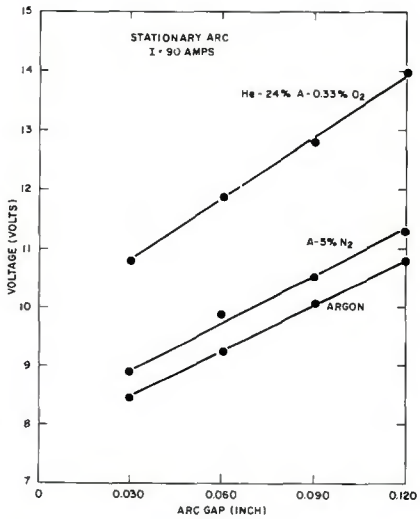

Fig. 7 — Variation in voltage as a function of arc gap for the different gases studied

The humped puddle configuration previously noted with the stationary arc weld is no longer present with the moving arc. It is assumed that the additional force in the pool due to the moving arc changes the pool motion, causing the puddle to solidify with the more normal contour appearance.

Shielding Gas

To demonstrate the importance of shielding gas, stationary welds were made using Argon, A-5% N_2, and He-24% A-0.33% O_2. The argon was chosen because of its standard use in welding; the A-N_2 to study the effects of a dissociating molecule in the arc discharge which has been mentioned as a means of improving weld penetration (Ref. 3); and the He-A-O_2 because it has also been mentioned as a means of increasing penetration. The results are quite dramatic as revealed in Table 5 and Fig. 6. The weld is extremely sensitive to the shielding gas which causes significant changes in heat input to the weld region.

Although the dissociation energy of nitrogen is only 7.9 eV, much of the energy in the arc is given to dissociating the N_2 molecule. This in turn requires a higher arc voltage to sustain the argon discharge and is evident in the results shown in Fig. 7. The energy absorbed from the arc by the nitrogen molecule is released when the molecules are reformed. If this recombination occurs at the surface of the weld metal, additional heat is given to the weld pool. This type of indirect heating from molecular dissociation, accounts for the major fraction of the heat input in the atomic hydrogen welding process. In this process, molecular hydrogen is dissociated as it is passed through an electric arc drawn between two tung-

Table 5 — Results of 10 Second Duration Stationary Arc Welds for Different Shielding Gases, Current = 91 A

	Argon				A−5% N_2				He−24% A−0.33%			
Arc gap mils	30	60	90	120	30	60	90	120	30	60	90	120
Width, in.	0.234	0.234	0.222	0.220	0.248	0.270	0.276	0.278	0.26	0.26	0.26	0.29
Depth, in.	0.048	0.038	0.036	0.040	0.068	0.068	0.056	0.054	0.07	0.11	0.13	0.10
Width/depth	4.87	6.16	6.19	5.50	3.61	3.96	4.94	5.15	3.7	2.4	1.9	2.9
Area × 100, sq. in.	0.69	0.67	0.68	0.72	1.12	1.07	1.03	1.06	1.24	2.03	2.90	2.22
Voltage, V	8.5	9.5	—	—	8.9	9.9	10.5	11.3	10.8	11.9	12.8	14.0

sten electrodes. When the plate to be welded is placed in the path of the atomic hydrogen coming through the arc, it cools the gas sufficiently to cause immediate recombination at the surface. The energy released due to the recombination, serves as the heat source for welding. Such an effect may account for the apparent increased heat input that is present in welding with the A-5% N_2 gas mixture.

The He-24% A-0.33% O_2 shielding gas shows even greater heat input and penetration than the A-5% N_2 weld. Because of the higher ionization potential of helium compared to argon (24.5 eV vs. 15.7 eV), the arc voltage necessary to sustain the He discharge is much higher than that of argon or the argon-nitrogen mixture for the same weld current. In addition, the dissociation of oxygen may produce effects similar to that for nitrogen, since it too is expected to be entirely dissociated. The dissociation energy of oxygen is only 5.09 eV.

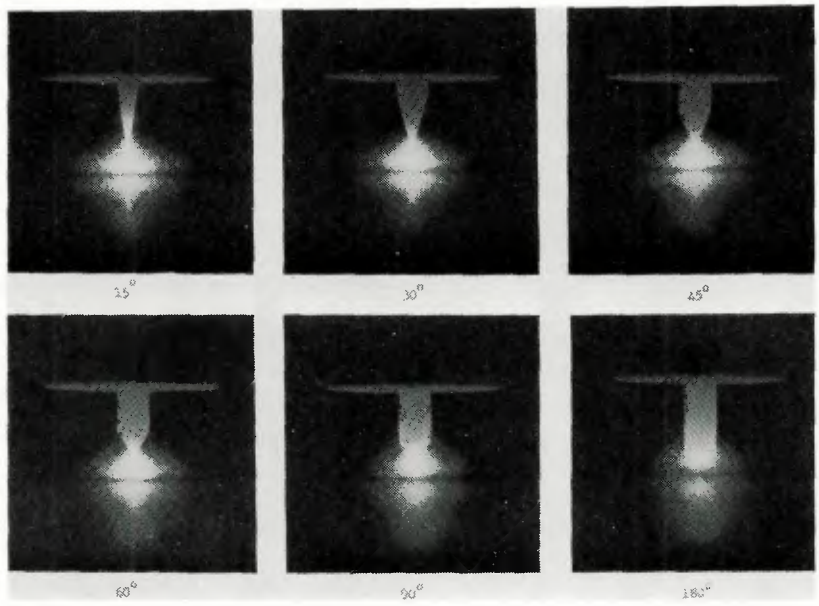

Fig. 8 — Effect of electrode angle on arc configuration in an argon discharge. I = 100 A, Arc gap = 0.080 in.

Electrode Configuration

Stationary and moving arc welds were made with a series of electrodes with an included angle varying between 15 and 180 deg. Each of the electrodes had a 0.005 in. flat tip. To study the effect of the "flatness," variations in the size of the flat were made for the 30 deg electrode. Photographs of the arc between a 3/32 in. thoriated tungsten electrode and a copper plate were taken with a polaroid camera using Type 58 film, and a No. 25 filter. The pictures shown in Fig. 8 reveal significant differences in the shape of the arc plasma. From observing the shape of the plasma it is not surprising to expect the changes in bead shape with variations in electrode geometry. The results of changes in the angle of the electrode tip are shown in Table 6, Table 7 and Fig. 9. These data indicate that the maximum area melted and maximum voltage occurred for the 30 and 45 deg electrode configuration. The depth-to-width ratio also indicated a maximum for these shaped electrodes. Erokhin (Ref. 4) has observed similar effects of a peak in the voltage and maximum penetration in his study of the influence of the tungsten cathode geometry on weld penetration. He explains his results by noting that the increased penetration with a sharpening of the electrode tip is accompanied by an increase in the arc jet pressure and the current density which he also measured on the anode surface. The reduction in penetration and arc pressure for the smaller angles (15 deg) is explained on the grounds that the highly concentrated incident energy at the anode, presumably causes the anode material to evaporate rapidly and build up a powerful anode plume. This lowers the direct arc pressure on the anode which results in less penetration.

Chihoski (Ref. 5) has reported on the effects of electrode shape on the arc while welding with aluminum. It is difficult to make comparisons with his work because in his study the voltage was kept constant. The increased arc pressure resulting from the more sharply pointed electrode is indicated (Ref. 5) to depress the molten puddle which would tend to increase the effective arc gap. In order to keep a constant voltage the electrode is thus allowed to extend below the work surface.

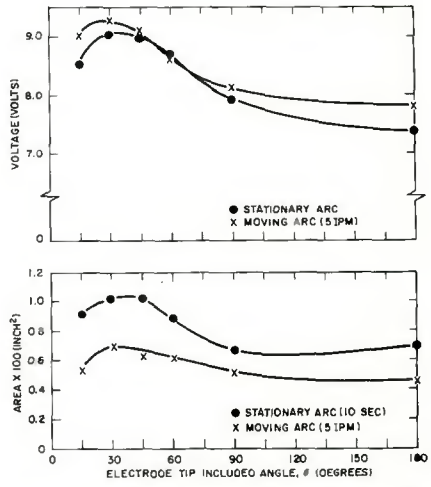

Fig. 9 — Effects of electrode tip configuration on voltage and area of weld bead with variation of tip angle. I = 90 A, arc gap = 0.035 in.

To explain the contradictory results of Savage et al (Ref. 6), which showed the trend of decreasing penetration with the reduction in tip angle, Spiller and MacGregor (Ref. 7) recently discussed the significant effect plate thickness has on such a

study. Their tests confirmed the Savage data where penetration is slight (under 30%), but indicated a reverse trend when thin plates were used and substantial penetration was obtained (above 70%). While Erokhin did not indicate the plate thickness he used in his study, the plates used in this study were ¼ in. thick and penetration less than 30%. The results of our work are in contradiction to the Savage study, and thus additional explanations and further effort are needed to explain these phenomena. Possibly, the difference in material studied may partially help to explain this anomoly.

The effect of electrode tip flatness on melt area and voltage is shown in Fig. 10. Although the width/depth ratio is essentially invariant to the flatness of the tip, the melt area decreases linearly as the tip flatness is increased, indicating a decrease in heat transfer efficiency with blunt tips. In Erokhin's studies a decrease in weld penetration was also found as the bluntness of the tip increased. This was attributed to the accompanying decrease in the measured arc pressure.

An often observed phenomenon is the umbrella-like halo that appears part way up the electrode and is separated from the main discharge as shown in Fig. 11a. These umbrella regions are occasionally accompanied by the growth of crystals or plates on the surface of the electrode. Chemical analyses of these particular crystals have shown them to be high in magnesium. A photograph of such a crystal is shown in

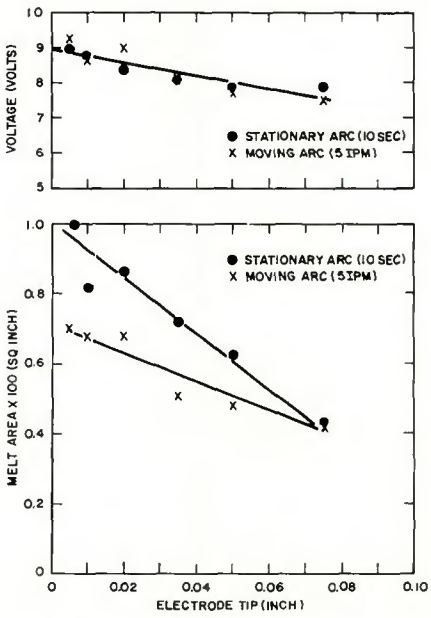

Fig. 10 — Effect of electrode tip configuration on voltage and area of weld bead with variation of tip flatness I = 90 A, arc gap = 0.035 in.

Table 6 — Effects of Electrode Configuration on Weld Bead Geometry and Arc Voltage for a Stationary Arc Weld. Dwell Time = 10 Seconds

Included angle, deg[a]	Voltage, V	Width in.	Depth in.	Area × 100, sq. in.
180	7.4	0.216	0.030	0.70
90	7.9	0.210	0.028	0.67
60	8.7	0.252	0.032	0.89
45	8.9	0.270	0.044	1.03
30	9.0	0.266	0.042	1.00
15	8.5	0.254	0.032	0.91
Tip Flatness in.[b]				
0.005	9.0	2.66	0.42	1.00
0.010	8.8	2.50	0.35	0.82
0.020	8.4	2.48	0.36	0.87
0.035	8.1	2.24	0.31	0.72
0.050	7.9	2.08	0.28	0.63
0.075	7.9	1.80	0.26	0.43

(a) 2% thoriated tungsten electrodes, 0.093 in. diam were used. Each of the electrodes had a 0.005 in. flat tip (except the 180 deg electrode).
(b) The electrodes used in this part of the study had a 30 deg included angle.

Table 7 — Effect of Electrode Configuration on Weld Bead Geometry and Arc Voltage for a Moving Arc, 5 ipm

Included angle, deg[a]	Voltage, V	Width, in.	Depth, in.	Area × 100, sq. in.
180	7.8	0.170	0.030	0.46
90	8.1	0.170	0.035	0.51
60	8.6	0.195	0.038	0.62
45	9.1	0.198	0.040	0.63
30	9.25	0.210	0.043	0.70
15	9.0	0.185	0.038	0.53
Tip Flatness in.[b]				
0.005	9.25	0.210	0.043	0.70
0.010	8.7	0.206	0.42	0.68
0.020	9.0	0.200	0.44	0.68
0.035	8.1	0.176	0.40	0.51
0.050	7.7	0.172	0.37	0.48
0.075	7.5	0.160	0.34	0.42

(a) 2% thoriated tungsten electrodes, 0.093 in. diam were used. Each of the electrodes had a 0.005 in. flat tip (except the 180 deg electrode).
(b) The electrode used in this part of the study had a 30 deg included angle.

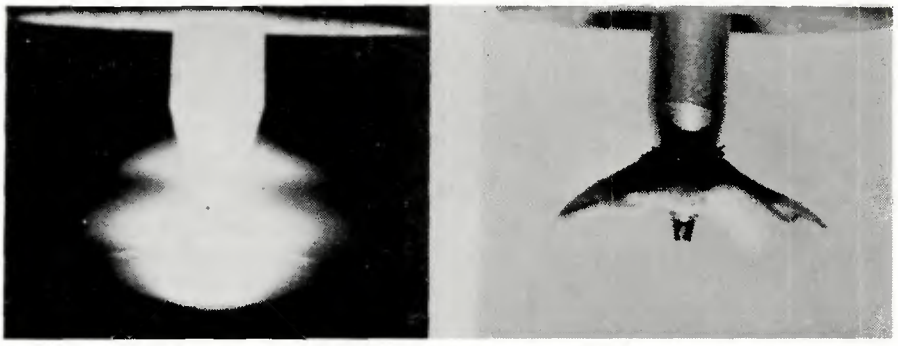

Fig. 11 — (a) Halo-effect occasionally observed accompanied by (b) growth of crystals or plates on the surface of the electrode

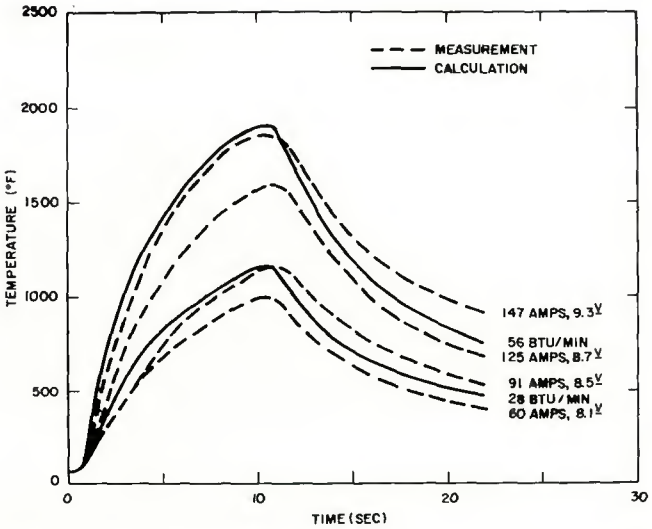

Fig. 12 — Calculated and measured temperatures at position T-2 for a stationary arc weld. Arc duration = 10 s., arc gap = 0.030 in.

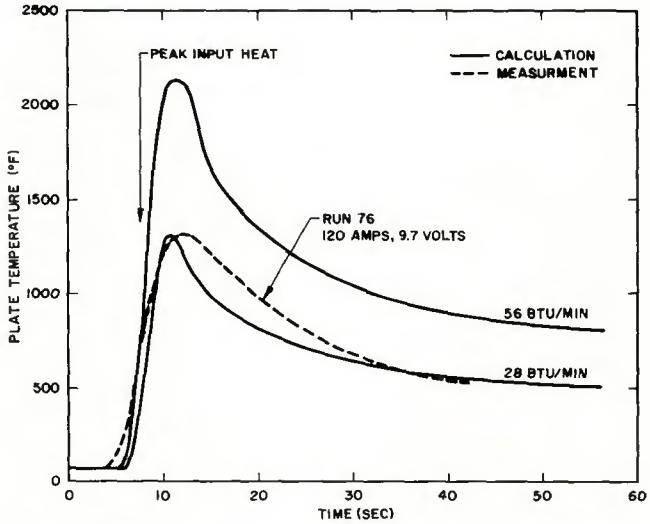

Fig. 13 — Plate temperature at position T-2 for an arc moving at 5 ipm, arc gap = 0.060 in.

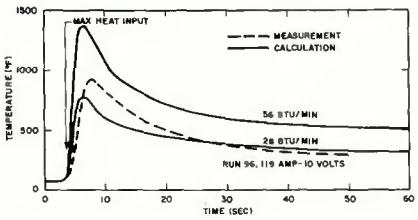

Fig. 14 — Plate temperature at position T-2 for an arc moving at 10 ipm, arc gap = 0.060 in.

Fig. 11b. Thus, it is concluded that the umbrella-like halo, shown in Fig. 11a, is the result of spectral lines emitted from exited atoms or ions which have been vaporized from the molten pool or from the electrode tip and tend to condense on the cooler region of the electrode.

Measurement and Calculation of Plate Temperature

Measurement

During the time welds were made for the parameter study, chromel-alumel thermocouples were attached to various points on the weld plates. The plate temperatures at each of these points were inferred from the graphic output of the voltage signal. An error of ± 100 F was estimated from the uncertainty in the zero setting and the limitations of the graphic interpretation of the absolute voltage. The results of these measurements are shown in Figs. 12-14. The peak temperature at each of the measured points is recorded in Tables 2-4.

Thermal Analysis Model

The temperature transients for both the stationary and the moving arc welds that are plotted in Figs. 12, 13, and 14 were computed using the finite element method of analysis, a complete description of which may be found, for example, in Zienciewicz (Ref. 8). The application of this method to the solution of transient heat conduction problems is outlined by Zienciewicz and Parekh (Ref. 9) and Wilson and Nickell (Ref. 10), among others. The program used to calculate the welding temperatures is featured by the use of the two-dimensional (planar or axisymmetric), biquadratic, isoparametric finite element (Ref. 9) and the modified Crank-Nicholson time integration scheme (Ref. 10). Liquid-solid phase change and the associated latent heat are included in the finite element thermal model by means of a recently-developed direct iteration procedure (Ref. 11), which is particularly applicable to alloy systems, in which melting and freezing occur over a range of temperatures.

Thermal analysis of the stationary arc welds was carried out by idealizing the plate to be circular. The thermal energy input from the arc is applied as a distributed heat flux at the center of the plate, and heat is assumed to be conducted axisymmetrically about the center (i.e., temperature varies only radially and through the thickness). For the time period of interest, this assumption is valid when computing temperature at the thermocouple locations (see Fig. 1b).

For the case of the moving arc welds, the determination of the transient three-dimensional temperature distribution is based on the attainment of quasistationary conditions, which result when (a) the heat source is moving at constant speed on a regular — in this case, straight — path, and (b) end effects resulting from initiation or termination of the heat source are neglected. The thermocouple locations are such that these conditions are met. The temperature distribution is then stationary with respect to a moving coordinate system whose origin always coincides with the center of the heat source. Thus, given the transient temperature distribution at any one section of the weldment normal to the direction of welding, the temperature at any other section, other than near the ends, can easily be determined. The problem therefore reduces itself to finding the two-dimensional unsteady temperature field at a section normal to the weld line. A planar analysis may be used for this purpose if the weld speed, relative to a characteristic thermal diffusion rate for the material, is sufficiently high that heat conducted ahead of the electrode is small. The weld speeds of 5 and 10 ipm used in the moving arc welds considered here meet this criterion.

A number of assumptions have been made in the calculations and it is important that these be emphasized.

1. The heat input distribution given in Fig. 15 is an estimate based on photographs of the arc and earlier published literature (Ref. 12). The half-width may be significantly different.

2. Conductivity above 1600 F was extrapolated to the melting temperature at 2400 F from measurements below this value. Above 2400 F the conductivity was assumed constant (Fig. 15). There is no experimental data above 1600 F for Alloy 600 (Ref. 13).

3. Heat transfer due to the motion of the molten pool was not considered, nor was any change in the shape of the surface of the pool considered. Furthermore, heat losses at

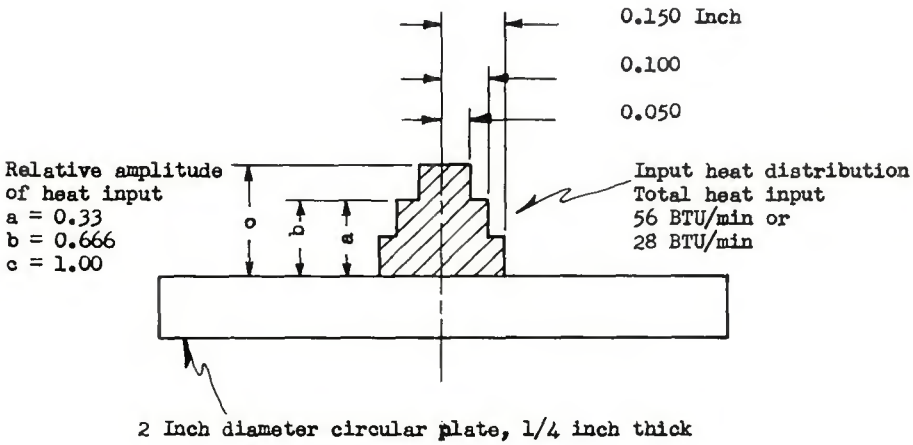

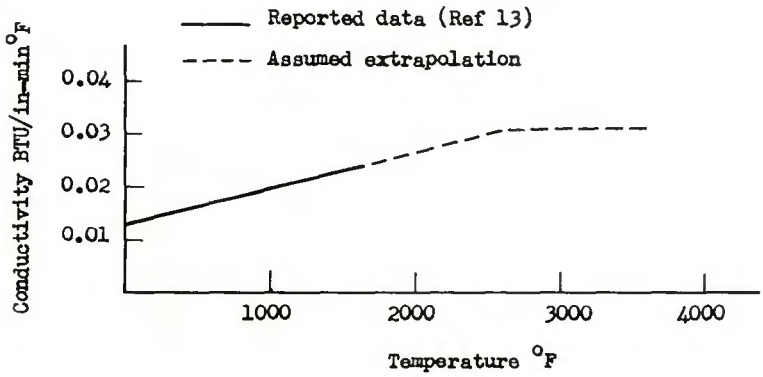

Physical Constants used for Alloy 600 (Ref 13)

Density = 8.43 gram/cm^3
Melt range = 2470°F - 2575°F
Specific heat at 70°F = 0.106 BTU/lb/°F

Fig. 15 — Input data for thermal analysis calculations

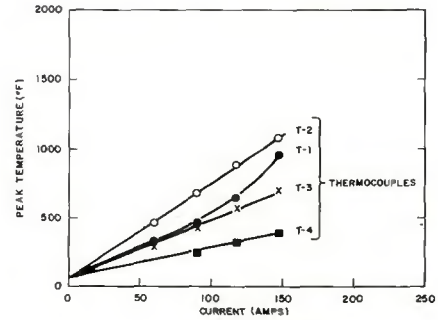

Fig. 16 — Peak plate temperature for a moving arc weld as a function of arc current. V = 10 ipm, arc gap = 0.030 in.

the boundary were assumed due to convection.

Analytical Results and Comparison With Experimental Data

Stationary Arc

Two stationary arc calculations with an assumed total heat input of 56 Btu /min and 28 Btu/min (1000 watts and 500 watts) respectively were performed, and the results compared to some experimental measurements in Fig. 12. As observed in this figure, the analysis predicts the general shape of the thermal cycle. The magnitude of the input heat used in the calculations was adjusted to agree with the peak temperature at thermocouple position T-2 for the two experimental cases shown. With such a heat input, the calculated temperatures during the cooling portion of the thermal cycle are lower than measured. They could have been adjusted to overlap the measured result by recalculating with a slightly modified heat input, but this would result in over-predicting the measured peak temperatures in the plate. Other input data such as boundary condition assumptions or heat transfer parameters must also be considered as a possible means of correcting for this ambiguity.

An interesting result that can be obtained from the analytical model is the effect of a changing heat input on the plate temperature, for example, at position T-2. From Fig. 12, it is observed that the temperature during the cool down period increased only 60-70% as the input heat is doubled. This is attributed to the depth of the weld puddle relative to the thickness of the plate. As the depth of the puddle is increased a greater fraction of the input heat begins to be conducted radially than through the thickness, resulting in the lower than expected temperature.

Moving Arc

Two moving arc calculations with an assumed heat input of 56 Btu/min and 28 Btu/min were performed for each of two weld speeds, 5 ipm and 10 ipm, respectively. The calculation, together with the experimental results are shown in Figs. 13 and 14. As observed in these figures the calculational shape of the thermal cycle is in poor agreement with the measured temperature during the initial rise and fall of the thermal cycle (t <30 seconds). Adjusting the input heat in the calculation to achieve agreement with the peak temperature at position T-2 does achieve reasonable agreement with the temperature for longer times. As in the stationary arc cases, adjusting the boundary conditions and material parameters is necessary to improve the correlation between measurement and calculation.

From Figs. 13 and 14 it is again concluded, as was with the stationary arc, that doubling the heat input (per linear inch) only increases the temperature at T-2 by approximately 70%. This is observed either by increasing the rate of heat input at a fixed welding speed or by decreasing the welding speed keeping the input heat constant.

In Fig. 16, the peak temperature of the measured points T_2, T_3 and T_4 was observed as linearly proportional to the input current. It was thought that the effects of a changing arc configuration (heat input distribution) with increased current would reveal a nonlinear relationship at these measured points. Except for point T-1, the thermocouples were sufficiently far from the source and the uncertainty larger than expected, to reveal any significant changes in heat distribution when the current was increased.

This was verified by comparing calculations with equal heat inputs, but with different spacial distributions. Typical results are shown in Fig. 17. While the resultant melt configuration was significantly different, the peak temperature differences measured at the thermocouple positions were within the experimental uncertainty of ±100 F. (Note, in this parameter change, the heat conduction was assumed constant.) Thus, an attempt to determine changes in weld bead shape with the use of thermocouples was not a very sensitive probe for this

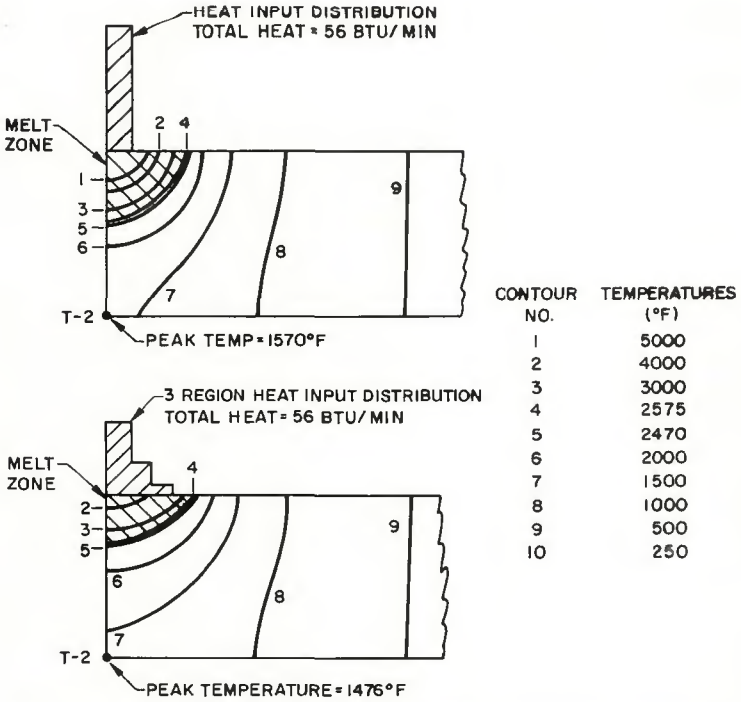

Fig. 17 — Comparison of calculated peak temperature isotherms after 10 s. of heat input (56 Btu/min) for two different heat distributions. The thermal conductivity was assumed constant for these calculations

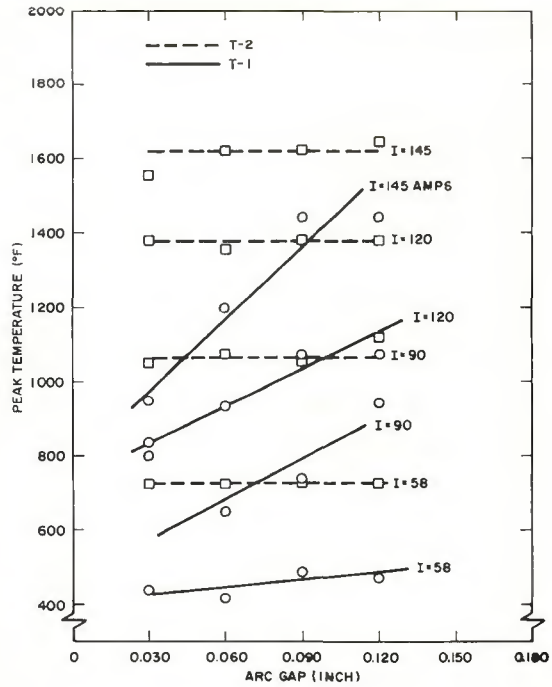

Fig. 18 — Peak plate temperature at position T-2 & T-1 as a function of arc gap and arc current. V = 5 ipm

thick plate condition. Improved experimental techniques in addition to employing more thermocouples would justify further effort.

A significant effect was found when comparing the peak temperature at position T-1 with varying arc gap as shown in Fig. 18. From these results it is concluded that the input heat distribution has widened as the arc gap increased. The change in the input heat distribution was insufficient to cause any observable change at the other thermocouple positions.

The most critical assumption made throughout this analysis is the neglect of the weld pool distortion and circulation. It is believed that the heat transfer through the weld pool is mainly due to circulation of metal within the pool (Ref. 14). Two mechanisms have been proposed which can give rise to this circulation: differences in interfacial surface tensions (Ref. 2), and magnetodynamic forces (Ref. 15). It is probable that both play an active part in changing the heat transfer characteristics of the liquid metal, but to what extent is presently uncertain. It is thus not expected that the analytical weld pool size and shape will agree with experimentally determined pool contour. Until this heat transfer mechanism is further explored and better understood, one will have to resort to a trial and error technique to adjust the effective thermal conductivity of the molten pool such that the results agree with experiment. This is not to be regarded as haphazard if such a scheme is able to predict a reasonable weld puddle size for various heat input conditions. This approach remains to be explored.

Conclusions

The data presented in this report describe a systematic study of the effects of weld parameters such as current, arc gap, torch speed, shielding gas and electrode shape on the weld bead geometry. The material studied was Alloy 600, in a thick plate configuration. Changes in the material, weld joint, and thickness of the plate could alter the weld bead geometry results that have been obtained during these tests. Thus, an analytical model was developed to provide an understanding as to what can be expected when changes are made in these quantities. As a result of this work, the following conclusions have been obtained:

1. In the case of a stationary arc weld, the cross section of the weld puddle revealed a humped contour configuration not usually observed. Such a configuration cannot be predicted by assuming a normal energy input distribution and standard heat conduction theory. Effects such as surface tension, arc jet forces, or Lorentz forces due to the current in the weld pool need to be resorted to in order to explain such phenomenon.

2. In the current range investigated (60 to 150 A) the width and depth of penetration increased linearly with weld current. These results are expected when the penetration is relatively small compared to the plate thickness as was the case in these experiments.

3. Decreasing the weld speed from 10 ipm to 5 ipm increased weld penetration but less than a factor of two. Calculational results verified these conclusions. At lower weld speeds a greater fraction of the energy input is transferred by conduction away from the weld puddle producing the relatively smaller puddle dimensions.

4. As the nominal power (V × I) increased with increased arc gap due to an increased arc voltage, the process efficiency decreased. This was noted for:

a) The case of the moving arc (5 ipm and 10 ipm). In these experiments the depth of penetration increased with decreased arc gap for low current, but had little effect for currents above 120 A.

b) A stationary arc. The depth of penetration was invariant to arc gap for currents below 100 A, but increased with decreasing arc gap for currents greater than 100 A.

5. He-24% A-0.33% O_2 shield gas significantly increased the heat input to the weld relative to using argon as a shielding gas. This is attributed to the higher ionization potential of helium which results in higher arc temperatures.

The use of nitrogen addition to the argon shield gas also increased the heat input to the weld area relative to pure argon. The use of a dissociative

gas such as N_2 is believed to increase the magnitude of the energy input to the weldment.

6. The depth, width, area, and arc voltage increased as the electrode tip angle was decreased from 180 to 30 deg. The trend reversed for the tip angle of 15 deg. This is contrary to published results on stainless steel plates. The size of the flat on the tip of the electrode also affected the final weld configuration. As the flat was decreased from 0.075 in. to 0.005 in. the area, depth, width, and voltage increased.

7. A finite element heat conduction model was developed to predict the plate temperature. However, additional effort is needed to further refine some of the assumptions employed in the model and to better estimate surface heat losses, liquid pool heat transfer characteristics, and the energy input distribution from the arc.

Acknowledgments

We would like to express our appreciation to G. N. Grimm, F. Salay, and F. E. Pawloski, Jr. for their assistance in conducting these experiments.

This report was prepared as an account of work sponsored by the United States Government. Neither the United States, nor the United States Atomic Energy Commission, nor any of their employees, nor any of their contractors, subcontractors, or their employees, makes any warranty, expressed or implied, or assumes any legal liability or responsibility for the accuracy, completeness or usefulness of any information, apparatus, product or process disclosed, or represents that its use would not infringe privately owned rights.

References

1. Chihoski, R. A. "The Rationing of Power Between the Gas Tungsten Arc and Electrode," *Welding Journal*, 49 (2), Feb., 1970, Res. Suppl. pp 69-s to 82-s.

2. Ishizaki, K. "Behavior of Molten Pool on Vertical Steel Plate Heated by Stationary TIG Arc," IIW Doc. SG 212-160-68, March, 1969.

3. Rybakov, Yu. V. and Novokreshchenov, M. M. "Influence of Nitrogen on the Gas Content of the Weld Metal and the Thermal Arc Power in the Argon Arc Welding of Steel EP 335," *Svar. Proiz.* No. 6, 1971.

4. Erokhin, A. A., Bukarov, V. A. and Ischenko, Yu. S. "Influence of Tungsten Cathode Geometry on Some Welding Arc Characteristics and Metal Penetration," *Svar Proiz*, No. 12, 1971.

5. Chihoski, R. A. "The Effects of Varying Electrode Shape on Arc, Operations, and Quality of Welds in 2014-T6 Aluminum," *Welding Journal*, 47 (5), May, 1968, Res. Suppl. pp 210-s to 222-s.

6. Savage, W. F., Strunck, S. S. and Ishikawa, J. "The Effect of Electrode Geometry in Gas Tungsten Arc Welding," *Welding Journal*, 44 (11), Nov., 1965, Res. Suppl. pp 489-s to 496-s.

7. Spiller, K. R. and MacGregor, G., "Effects of Electrode Vertex Angle on Fused Weld Geometry in TIG Welding," *Proc. of the Conf. on Advances in Weld Processes*, 14-16 April, 1970, The Weld Inst., Abington Hall, Cambridge, 1971.

8. Zienciewicz, O. C., *The Finite Element Method in Engineering Science*, McGraw-Hill, London, 1971.

9. Zienciewicz, O. C. and Parekh, C. J., "Transient Field Problems: Two-Dimensional and Three-Dimensional Analysis by Isoparametric Finite Elements," *Intl. J. Numerical Methods Engr.*, Vol. 2, 1970.

10. Wilson, E. L. and Nickell, R. E., "Application of the Finite Element Method to Heat Conduction Analysis," *Nuclear Engr. and Design*, Vol. 4, 1966.

11. Friedman, E., "A Direct Iteration Method for the Incorporation of Phase Change in Finite Element Heat Conduction Programs," WAPD-TM-1133, Bettis Atomic Power Laboratory, March, 1974.

12. Nester, O. H., "Heat Intensity and Current Distribution at the Anode of High Current, Inert Gas Arcs," *J. App. Physics*, Vol. 33, May, 1962.

13. Huntington Alloy Products Division, "Inconel Alloy 600," 3rd Edition, 1969.

14. Boughton, P., "High Precision Pulsed TIG Welding," *Proc. of the Conf. on Advance in Weld Processes*, 14-16 April, 1970, The Weld Inst., Abington Hall, Cambridge, 1971.

15. Woods, R. A. and Milner, D. R., "Motion in the Weld Pool in Arc Welding," *Welding Journal*, 50 (4), April 1971, Res. Suppl. pp 163-s to 173-s.

Five AWS Books On Topics of Interest

C5.1-73, Recommended Practices for Plasma-Arc Welding and **C5.2-73, Recommended Practices for Plasma-Arc Cutting** examine the how-to-do aspects of these processes. The characteristics of the processes are discussed, the various components of the equipment are described and data for guiding prospective users in the setting up and use of the equipment are presented.

C5.3-74, Air Carbon-Arc Gouging and Cutting describes the air carbon-arc cutting process and supplies detailed information on equipment, base metals, areas of application, and safety precautions. In addition, it offers helpful suggestions on techniques for gouging, severing, beveling, and washing off excess metal. A special "trouble shooting" section, providing solutions to various problems, is also included.

C5.4-74, Recommended Practices for Stud Welding is intended to serve as a basic guide for those interested in attaching fasteners by arc, capacitor-discharge, or drawn-arc stud welding. Included in the publication are stud and equipment descriptions, suggested qualification procedures and inspection methods, and recommended practices for welding. Following these suggested measures will permit the efficient use of studs in applications involving aircraft and aerospace fabrication, appliances, automotive vehicle manufacturing, boilers, bridge and building construction, equipment manufacturing, hardware, metal furniture, railroads, and shipbuilding.

Although compiled primarily for those concerned with titanium piping and tubing, the up-to-date information contained in **D10.6-73, Gas Tungsten-Arc Welding of Titanium Piping and Tubing,** will be of interest to anyone who welds titanium. Topics covered include: filler metal, joint preparation, procedures and technique, and weld quality tests.

Prices*

C5.1-73, Recommended Practices for Plasma-Arc Welding	$4.00
C5.2-73, Recommended Practices for Plasma-Arc Cutting	$2.00
C5.3-74, Air Carbon-Arc Gouging and Cutting	$3.00
C5.4-74, Recommended Practices for Stud Welding	$3.00
D10.6-73, Gas Tungsten-Arc Welding of Titanium Piping & Tubing	$2.00

**Discounts: 25% to A and B members; 20% to bookstores, public libraries and schools; 15% to C and D members. Add 4% sales tax in Florida.*

Send your orders for copies to the American Welding Society, 2501 N.W. 7th Street, Miami, Florida 33125.